Growth of Single Crystalline TiO$_2$ Nanorods as a Photoanode for Dye-Sensitized Solar Cell

Chang Woo Kim[1,2], Sohyun Ji[1], Dong In Kang[1] and Young Soo Kang[1] *

[1]Korea Center for Artificial Photosynthesis and Department of Chemistry, Sogang University, #1 Shinsu-dong, Mapo-gu, Seoul 121-742, Republic of Korea

[2]McKetta Department of Chemical Engineering, The University of Texas at Austin, Austin, Texas 78712, USA

yskang@sogang.ac.kr

Keywords: Dye-sensitized solar cells, Photoanode, Single crystal, TiO$_2$, Nanorod

Abstract. Single crystal TiO$_2$ nanorod (TNR), aligned vertically and packed with the length up to 10 μm on the surface of FTO glass, are prepared hydrothermal method, without any surfactant materials. By adjusting reaction time and concentration of titanium precursor solution, the morphology of TNRs is controlled and result in 20-50 nm of diameters, 4-10 μm length and the inter-distance between TNRs are approximately 3.8 nm. Morphology-controlled TNR arrays are applied to a photoanode in photovoltaic cell. photo-conversion efficiency of Packed TNRs with 10 μm length reached 4.2%.

Introduction

Photovoltaic solar cells have been received huge attention with the growing demands of green and clean energy [1]. Especially, since Oregan and Gratzel reported mesoporous TiO$_2$ electrode dye sensitized solar cells (DSSCs) in 1991[2] the related works have been widely reported for the enhanced performance. For enhancing DSSCs performance, several things need to be considered such as dyes with high adsorption coefficient and electrolyte with more stability [3,4]. Among these, the study has been especially focused on the functions of the fast electron transport and high electron collecting ability. Until now, Nanocrystalline TiO$_2$ electrode with 12 μm-thick film ,using FTO glass as a substrate is the most general photoelectrochemical electrode. Although its has large surface area, the electron diffusion in nanoparticulate films was interrupted because of electrons are trapped at the contacts between nanoparticles.

Study about vertically aligned single crystalline semiconductor nanorod/nanowire electrodes receive huge attention from researchers because those electrodes provide direct electrical pathways for photogenerated electrons [8-16]. Several materials such as TiO$_2$ and ZnO are tried to get possessed nanorod/nanowire sturucture. The highest solar to electricity conversion efficiency has been achieved by [10 0] oriented multichannel ZnO nanowire array, which reached to 6.15% [21]. In ZnO-based DSSCs electrodes such as 1-dimensional (1D) crystalline nanorod or nanowire arrays, has poor photo conversion efficiencies because of the instability of ZnO in acidic dye solution and low surface area .approximately 2% less compared to those made from TiO$_2$ [17-20]. Polycrystalline TiO$_2$ nanotube array films can reduce the recombination rate and TiO$_2$ nanotube electrodes show slightly faster electron transport rate in DSSCs. However the fabrication of TiO$_2$ nanotube array films is very challenging because of a series of steps such as Ti film deposition, an anodization step, and sintering, which reduce the conductivity of the FTO layers [22-24]. Although there are some articles researched on synthesis of vertically oriented single-crystalline TNRs or TiO$_2$ nanowires using a variety of synthesizing methods [25,26] , those electrodes could not produce remarkable enhanced performance in their DSSCs because of their low roughness factor, which results in insufficient short circuit current. Roughness factor relate with surface area of electrode which can affect amount of adsorbed dye on the surface of electrode. Therefore, for better performance, the roughness factor needs to get larger. Considering roughness factor, closed packed single crystalline rutile TiO$_2$ with 1D longer

length provides larger surface area and increases their roughness factor. Recently, several strategies have been tried for enhancing the efficiency of DSSCs using 1D TNRs photoanodes, such as combination with 3D structures [27,28] or etching to porous nanorod arrays [29].

In this study, we demonstrated simple hydrothermal methods [30] for the controlled morphology of closed packed single crystalline rutile TNR arrays up to 10 μm length on FTO glass. Controlling the morphology, length, and diameter of TNRs are tried to get the highest efficiency of DSSC electrode. Possible mechanism for the formation of TNRs was suggested and solar light to electricity conversion efficiency of single crystalline TNR electrodes with many different morphology, length, and diameter has been studied.

Experimental

Synthesizing vertically aligned TNRs on FTO coated substrate

A 20 mL of sealed teflon reactor was filled with 4.5 mL of hydrochloric acid (37 wt%) and 4.5 mL of deionized water. After the solution was stirred for 10 min, 1.5 mL of titanium butoxide (97%, Aldrich) was added into the solution with stirring for another 10 min. And then 6 mL of toluene and 1.5 mL of titanium tetrachloride (final: 1 M titanium tetrachloride in toluene) were added with stirring for another 10 min. FTO substrates were put in solution composed with deionized water, acetone, and 2-propanol (V: V: V =1: 1: 1) and sonicate for 10 min. The substrate was dried with a nitrogen gas flowing. For a thin TiO_2 layer with 20 nm thick deposited on the FTO coated glass, TiO_2 layer was coated on FTO by using spin coater with 2 wt% of titanium (IV) bis(ethyl acetylaceto) diisopropoxide in butanol (1-butanol) solution and then sintered the FTO glass in furnace at 450 °C for 4 h. TiO_2 layered FTO glass was placed vertically on side wall. The reactor carried hydrothermal reaction out at 180 °C from 1 to 8 h and then cooled to room temperature. The TNRs samples were washed with ethanol and DW(deionized water) subsequently, and dried with a nitrogen stream.

Assembly of DSSCs with rutile TNRs photoanode

For assembly of DSSCs, the prepared samples were put in 0.3 mM N-719 dye (Solaronix Inc., Switzerland) solution of tert-butanol: ACN (V: V: =1: 1) for 24 h to finish the dye adsorption [24,31].The counter-electrode was prepared as 100 nm of Pt on a FTO substrate by sputter. It is necessary to place a 25 μm thick SX-1170 spacer (Solaronix Inc., Switzerland) between the TNR and Pt counter-electrode for protecting TNRs from the heat pressing and injecting redox electrolyte. A liquid electrolyte for DSSC was prepared using MPN-100 (Solaronix, Inc., Switzerland). This electrolyte was injected into the space between the anode and the cathode. The photovoltaic properties of DSSCs were monitored by recording the photocurrent-voltage (I-V) curves with active sample areas of 0.48 cm^2 under simulated 1 sunlight with 100 mW cm^{-2} of A.M 1.5 (300 W Oriel Solar Simulator).

Characterization and Photovoltaic Performance Measurement of DSSCs

Operating at 30 kV and 15 mA at a scanning rate of 0.02 deg. step-1 in the 2θ range of 10° ≤ 2θ ≤ 80°, XRD with Cu Kα radiation (λ = 1.54056 Å) from a Rigaku MiniFlex II desktop For characterize the crystal structure of TNR, X-ray was used. Microscopic observation of TNR and their film was conducted with a scanning electron microscope (SEM, Cold Field-Emission Scanning Electron Microscope Hitachi S-4300) and a transmission electron microscope (TEM, JEOL, JEM-2100F, operated at 200 keV).

After careful calibration with a Si reference cell (PV Measurements Inc.), the photovoltaic performance of a DSSCs was measured under a 1-sun condition (100 mW cm^{-2}, AM 1.5 G) using a solar simulator (Newport) equipped with a 300-W Xe lamp and a Keithley (Model 2400) source meter. A black mask with a 0.16 cm^2 aperture was laid on the cells during irradiation. The DSSCs were measured both in the dark and under illumination in the 1-MHz- to 200-mHz-frequency range while an AC voltage of -0.70 V was applied using a DIGITAL-AVR potentiostat (UPS BANK, Korea) operating in the two-electrode mode. The IPCE measurement was conducted by QEX7 (PV

Measurements, Inc.) with a chopping speed of 10 Hz. To identify the chemical composition on the surface of the film, X-ray photoelectron spectroscopy (XPS, MultiLab 2000) analyses were performed and calibrated by the binding energy of C 1s 284.6 eV. Nitrogen adsorption/desporption isotherms were measured with an automated QUADRASORB 'SI' analyzer of Quantachrome Instruments at 77 K.

Results and Discussion

Fig. 1(a-e) show the top viewed- and cross sectional SEM images of the as-synthesized TNR array films. With the reaction times for 1-8 h, samples show significant uniformity and compact array of aligned nanorods with tetragonal crystallographic planes. This result shows that by increasing reaction time, the length of TNRs and the diameter of square shape TNRs can be increased. During the reaction process, TNRs nucleate and grows toward [001] axis direction, which was monitored by XRD, TEM and SAED. TNR peaks are well matched with the XRD database of tetragonal rutile (JCPDS no. 88-1175). The enhanced (001) peak in Fig. 1(f) XRD pattern demonstrates that the well single crystallized TNRs are grown vertically on the FTO coated glass Also the diffraction peaks such as (110), (111), and (211) are disappeared on spectrum, this also indicates that TNRs were grown in the [001] direction. The results of the vertically grown TNRs with 10 μm on FTO glass were shown in Fig. 1(e) and 2. Consistent with the XRD data, in TEM and SEAD study, TNRs have (110) inter-plane distance of 0.325 nm and the TNRs are vertically grown along the (110) crystal plane with the [001] direction from the lattice fringe and SAED pattern. Additionally, they indicate that TNRs are completely crystalline along their entire lengths toward [001] direction.
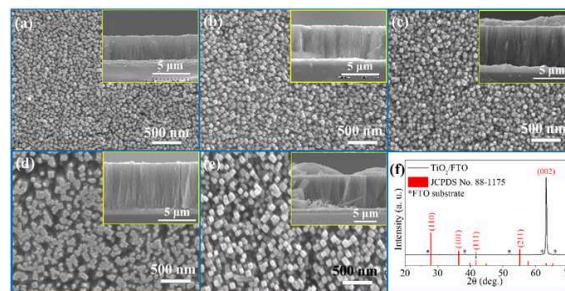

Figure 1. Top view and cross sectional SEM images of vertically grown TNR samples on FTO coated glass at 180 ^{o}C with different reaction times: (a) 1 h, (b) 2 h, (c) 3 h, (d) 4 h, and (e) 8 h. (f) is a typical XRD pattern of the nanorod array film on FTO as shown in (e).
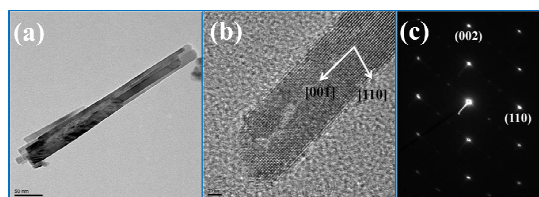

Figure 2. TNRs vertically grown on FTO glass; (a) TEM image of the TNRs, (b) HRTEM image of the TNRs, (c) SAED pattern.

By the hindrance which is triggered from the reduced space between TNR**s**, the closely-packed TNRs stop growing. The average length of TNR was increased from 4 μm for 1 h of reaction to 10 μm long for 8 h of reaction. When the growth time get over 8 h, caused by a equilbrium between growth rate and dissolution rate, there is no further increase in the diameter and length of nanorods. At the beginning of the reaction, the concentration of the titanium salt is high enough to grow the TNRs. The growth system of TNR**s** approaches equilibrium as the crystal growth rate starts to decrease at the longer reaction time. Due to the role of TiCl$_4$, the longer nanorods are synthesized than the previously reported by Liu et al. [26]. TiCl$_4$ could control the length, diameter and packing density of the TNR arrays. First, the addition of TiCl$_4$ remarkably increased the ionic strength of the reaction solution and the enhanced ionic strength through electrostatic screening triggers formating smaller crystals. And as

a result of this, the possibility of colliding with neighboring nanorods is reduced. Second, Cl⁻ ions can adsorb onto the side (110) facet selectively and play a important role for a diffusion barrier for the growth of side facet suppressing the diffusion of the precursors to the side surface of TNRs [37,38]. Hence by TiCl$_4$ addition, rate of diameter growth is retareded. and longer TNRs can be formed. In Fig. 3, this suggestion can be confirmed by changing the concentration of the initial precursor in the reaction solution. The diameter of nanorods could be increased by reducing the volume of TiCl$_4$ in the reaction solution from 1.5 mL to 0 mL and some part of the tetragonal shape of TNRs change into the circular shape by further reducing the amount of Cl⁻ in the reaction solution because the decreasing concentration of Cl⁻ ions triggers the formation of larger crystals and varies square shape of nanorod cross section to circular shape due to reduce ionic strength
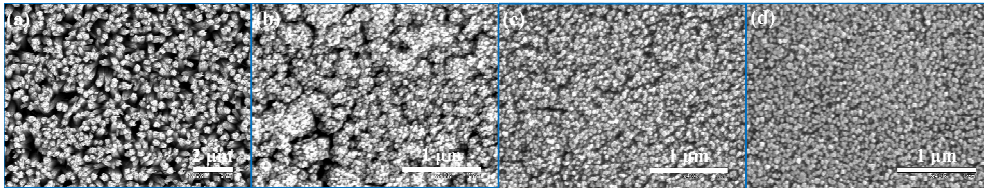
Figure 3. SEM images of vertically grown TNR array on FTO substrate at 180 $^{\circ}$C for 4 h with diverse amounts of TiCl$_4$ in the reaction solution. (a) 0 mL, (b) 0.6 mL, (c) 0.9 mL, and (d) 1.2 mL of TiCl$_4$.
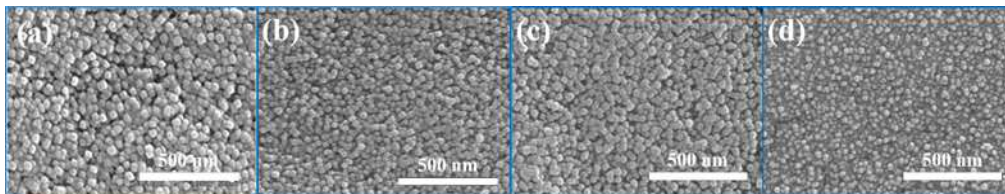
Figure 4. SEM images of vertically oriented TNR**s** array on TCO substrate at 180 °C for 4 h with diverse amounts of titanium butoxide in reaction solution; (a) 0 mL, (b) 0.5 mL, (c) 1.0 mL, and (d) 1.5 mL of titanium butoxide.

Fig. 4 shows that the density of the TNRs could be changed by increasing the initial volume of titanium butoxide in the reaction solution from 0 to 1.5 mL. Decreasing of the quantity of titanium butoxid induces the reduction of the nucleation density, and this leads the decreased packing density of the TNRs. When for the titanium source, there is only TiCl$_4$, the width of the TNRs increases rapidly up to average value of 300 nm diameters and the nanorod with 300 nm diameters is consisted of a bundle of TNRs with 20 - 30 nm diameters. This is resulted from a higher chemical reactivity of TiCl$_4$, which leads to the larger size of the seed particles for the nucleation. The increase of the amount of titanium butoxide in a solution which composed with 1.5 mL of TiCl$_4$ (1 M in toluene), toluene 6 mL, 4.5 mL of deionized water and 4.5 mL of HCl, prevents the formation of a bundle of TNRs and the increase of the TNRs diameter by the decreased reactivity of Ti^{4+}. Therefore, an increase in diameter of nanorods induces decrease the packing density of the nanorods, which triggers the decrease of dye adsorption, despite the longer length. But the rapid growth in length compensates the lower surface area caused by enlarging the diameter of TNRs in our experimental condition.

To get detailed elemental information on the surface of the as-obtained TNR array films, the typical XPS spectra of the Ti 2p and O 1s were checked as shown in Fig. 5 The XPS spectrum of Ti 2p only shows doublet peaks at 458.6 eV (Ti 2p3/2) and 464.2 eV (Ti 2p1/2), corresponding to the characteristic Ti^{4+} oxidation state in titania lattice [32]. For the O 1s core level spectrum, it contains a main peak at low binding energy of 529.8 eV and another peak at high energy binding energy of 531.5 eV, which comes from the crystal lattice oxygen (O2⁻) of Ti–O–Ti and the oxygen in hydroxyl groups (–OH) from the surface adsorbed water on TiO$_2$ surface, respectively [32-34]. The presence of surface hydroxyl groups is related with adsorption ability photosensitive dyes such as N719 sensitizer [35,36].
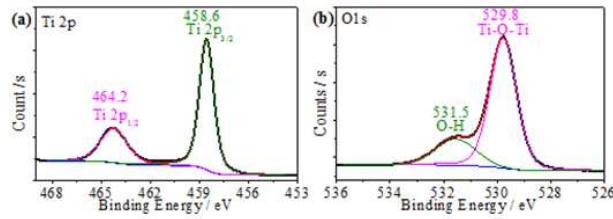
Figure 5. The typical XPS spectra of the as-obtained sample TiO$_2$/FTO film: (a) Ti 2p; (b) O 1s. The black curves correspond to the experiment data, and they were fitted with the colored curves (including background, dissociated peaks, and peak sum) using an XPS fitting program (XPSPEAK41).
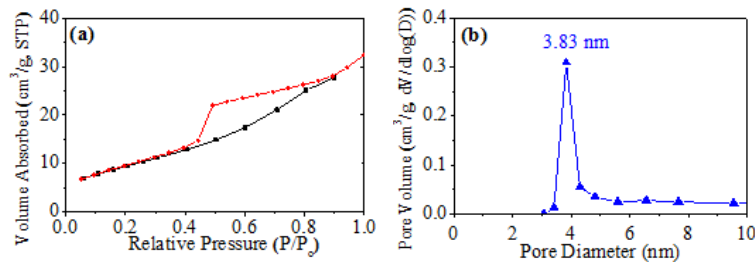

Figure 6. TNRs vertically grown on FTO coated glass with 8 h of reaction time (a) N2 adsorption/desorption isotherms of vertically oriented TNRs array and (b) N2 adsorption/desorption isotherms of pore size distribution of vertically oriented TNRs array.

The Brunauer-Emmett-Teller (BET) specific surface area of the TNRs with 10 μm is determined as 29 m^2 g^{-1} in Fig. 6(a). The TNRs provide less surface area for adsorbing dyes than the P25 film with ~55 m^2 g^{-1} of surface areas although the TNRs possesses higher crystallinity [39]. Fig. 6(b) demonstrates that the average pore diameter of the TNRs array is determined as 3.83 nm by the nitrogen adsorption/desorption measurement, which suggests that the average inter-distance between the TNRs is determined as 3.83 nm. For further application, we have checked light-to-electricity conversion efficiency of single crystalline TNRs electrode with diverse morphology, length, and diameter in DSSC device. Fig. 7 shows the I-V characteristics of samples synthesized by different reaction time under AM 1.5 illumination. Additional photovoltaic parameters are shown in Table 1. A photoconversion efficiency of 1.4% is accomplished for 4 μm length TNR arrays, with an open circuit voltage (Voc) of 0.77 V, fill factor (FF) of 0.63, short circuit current density (Jsc) of 2.8 mA cm^{-2} and Photoconversion efficiencies of 6.0 and 10.0 μm lengths of TNR arrays are achieved at 2.8% (Voc = 0.77 V, Jsc = 6.3 mA cm^{-2}, FF = 0.58), and 4.2% (Voc = 0.75 V, Jsc = 11.5 mA cm^{-2}, FF = 0.54), respectively. The increased surface area enhances the solar cell performance by the increased amount of dye absorption, corresponding to decrease of the packing density per unit area of the TNR electrode.
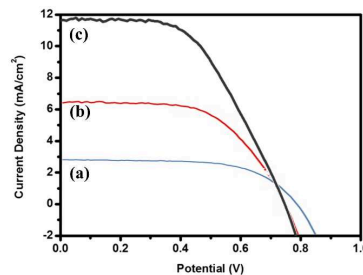

Figure 7. I-V curves of the vertically oriented TNRs array grown on FTO substrate with different lengths based dye sensitized solar cells under 1 sun illumination (AM 1.5, 100 mW cm^{-2}). (a) 4, (b) 6, and (c) 10 μm lengths of TNRs arrays.

Summary

Vertically aligned, closed packed single crystalline rutile TNR arrays up to 10 μm length on FTO substrate was prepared by low-temperature hydrothermal method. For enhancing of the cell efficiency, several growth parameters such as the growth time and initial reactant concentration were selectively chosen to produce TNRs up to 10 μm length. A light to electricity conversion efficiency could be reached up to 4.2% by employing 10 μm length TNR as the photoanode in a DSSC

References

[1] J. P. Han, E. J. Lee, Y. W. Han, T. H. Lee, D. K. Moon, J. Ind. Eng. Chem. 36 (2016) 44-48.

[2] B. Oregan, M. Grätzel, Nature, 353 (1991) 737-740.

[3] M. Liang, J. Chen, Chem. Soc. Rev. 2013, 42, 3453-3488.

[4] M. Sánchez Carballo, M. Urbani, A. Kumar Chandiran, D. González-Rodríguez, P. Vázquez, M. Grätzel, M. K. Nazeeruddin, T. Torres, Dalton Trans. 43 (2014) 15085-15091.

[5] A. Solbrand, H. Lindström, H. Rensmo, A. Hagfeldt, S. E. Lindquist, S. Södergren, J. Phys. Chem. B 101 (1997) 2514-2518.

[6] J. van de Lagemaat, N. G. Park, A. J. Frank, J. Phys. Chem. B 104 (2000) 2044-2052.

[7] J. Villanueva-Cab, S.-R. Jang, A. F. Halverson, K. Zhu, A. J. Frank, Nano Lett. 14 (2014) 2305-2309.

[8] A. U. Pawar, C. W. Kim, M. J. Kang, Y. S. Kang, Nano Energy 20 (2016) 156-167.

[9] L. E. Greene, B. D. Yuhas, M. Law, D. Zitoun, P. D. Yang, Inorg. Chem. 45 (2006) 7535-7543.

[10] G. K. Mor, K. Shankar, M. Paulose, O. K. Varghese, C. A. Grimes, Nano Lett. 6 (2006) 215-218.

[11] L. E. Greene, M. Law, B. D. Yuhas, P. D. Yang, J. Phys. Chem. C 111 (2007) 18451-18456.

[12] K. Zhu, N. R. Neale, A. Miedaner, A. J. Frank, Nano Lett. 7 (2007) 69-74.

[13] K. S. Leschkies, R. Divakar, J. Basu, E. Enache-Pommer, J. E. Boercker, C. B. Carter, U. R. Kortshagen, D. J. Norris, E. S. Aydil, Nano Lett. 7 (2007) 1793-1798.

[14] Z. Wang, S. Ran, B. Liu, D. Chen, G. Shen, Nanoscale 4 (2012) 3350-3358.

[15] W. Guo, C. Xu, X. Wang, S. Wang, C. Pan, C. Lin, Z. L. Wang, J. Am. Chem. Soc. 134 (2012) 4437-4441.

[16] H. Yu, J. Pan, Y. Bai, X. Zong, X. Li, L. Wang, Chem. Eur. J. 19 (2013) 13569-13574.

[17] J. B. Baxter, E. S. Aydil, Appl. Phys. Lett. 86 (2005) 053114.

[18] M. Law, L. E. Greene, J. C. Johnson, R. Saykally, P. D. Yang, Nat. Mater. 4 (2005) 455-459.

[19] C. K. Xu, P. Shin, L. L. Cao, D. Gao, J. Phys. Chem. C 114 (2010) 125-129.

[20] A. B. F. Martinson, J. W. Elam, J. T. Hupp, M. J. Pellin, Nano Lett. 7 (2007) 2183-2187.

[21] D. He, X. Sheng, J. Yang, L. Chen, K. Zhu, X. Feng, J. Am. Chem. Soc. 136 (2014) 16772-1677.

[22] G. K. Mor, K. Shankar, M. Paulose, O. K. Varghesen, C. A. Grimes, Nano Lett. 5 (2005) 191-195.

[23] G. K. Mor, K. Shankar, M. Paulose, O. K. Varghesen, C. A. Grimes, Appl. Phys. Lett. 91 (2007) 152111.

[24] C. W. Kim, S. P. Suh, M. J. Choi, Y. S. Kang, Y. S. Kang, J. Mater. Chem. A 1 (2013) 11820-11827.

[25] X. Feng, K. Shankar, O. K. Varghese, M. Paulose, T. J. Latempa, C. A. Grimes, Nano Lett. 8 (2008) 3781-3786.

[26] B. Liu, E. S. Aydil, J. Am. Chem. Soc. 131 (2009) 3985-3990.

[27] S. S. Mali, H. Kim, C. S. Shim, P. S. Patil, J. H. Kim, C. K. Hong, Sci. Rep. 3 (2013) 3004.

[28] Z. Haider, Y. S. Kang, ACS Appl. Mater. Inter. 6 (2014) 10342-10352.

[29] M. Lv, D. Zheng, M. Ye, J. Xiao, W. Guo, Y. Lai, L. Sun, C. Lin, J. Zuo, Energy Environ. Sci. 6 (2013) 1615-1622.

[30] H. G. Cha, J. Song, H. S. Kim, W. Shin, K. B. Yoon, Y. S. Kang, Chem. Commun. 47 (2011) 2441-2443.

[31] C. W. Kim, M. J. Choi, S. Lee, H. Park, B. Moon, Y. S. Kang, Y. S. Kang, J. Phys. Chem. C 119 (2015) 24902-24909.

[32] J. Li, J. Xu, J. Huang, CrystEngComm 16 (2014) 375-384.

[33] J. Y. Zheng, T. K. Van, A. U. Pawar, C. W. Kim, Y. S. Kang, RSC Adv. 4 (2014) 18616-18620.

[34] J. Y. Zheng, G. Song, J. Hong, T. K. Van, A. U. Pawar, D. Y. Kim, C. W. Kim, Z. Haider, Y. S. Kang, Cryst. Growth Des. 14 (2014) 6057-6066.

[35] A. S. Vuk, R. Jese, B. Orel, G. Drazic, Int. J. Photoenergy 7 (2005) 163-168.

[36] K. E. Lee, M. A. Gomez, S. Elouatik, G. P. Demopoulos, Langmuir 26 (2010) 9575-9583.

[37] H. G. Yang, C. H. Sun, S. Z. Qiao, J. Zou, G. Liu, S. C. Smith, H. M. Cheng, G. Q. Lu, Nature 453 (2008) 638-641

[38] J. Chen, H. B. Yang, J. Miao, H. Y. Wang, B. Liu, J. Am. Chem. Soc. 136 (2014) 15310-15318.

[39] T. Fröschl, U. Hörmann, P. Kubiak, G. Kučerová, M. Pfanzelt, C. K. Weiss, R. J. Behm, N. Hüsing, U. Kaiser, K. Landfester, M. Wohlfahrt-Mehrens, Chem. Soc. Rev. 41 (2012) 5313-5360.